

## Photoionization from Outer Atomic Subshells. A Model Study

JOHN W. COOPER  
*National Bureau of Standards, Washington, D. C.*  
 (Received June 6, 1962)

Calculations of photoionization cross sections are reported which emphasize the spectral range (from threshold to  $\sim 150$  eV above it) where the bulk of the optical oscillator strength is distributed and where the cross sections are large but experimental evidence is scarce. We have used as a model the light absorption by a single electron moving in a potential similar to the Hartree-Fock potential appropriate to the outer subshell of each atom. Data are reported for the rare gases He, Ne, Ar, and Kr, for Na, and for the closed-shell ions Cu<sup>+</sup> and Ag<sup>+</sup>. Sum rules are used to analyze the oscillator strength spectral distribution and to attempt extrapolations to still higher energies. The results suggest a classification of atomic subshells into two types with fundamentally different spectral distributions of oscillator strength. One type consists of the subshells 1s, 2p, 3d, 4f, with nodeless radial wave functions, the other type includes all remaining subshells. The present calculations are regarded as a first approximation to be improved upon by taking into account configuration interaction.

### I. INTRODUCTION

ALTHOUGH atomic photoionization has been studied extensively in the x-ray region<sup>1</sup> little has been done at lower energies<sup>2</sup>; i.e., in the range from threshold to 100 eV. While quantum mechanics provides us with an explicit formulation in terms of the initial and final states of the atomic system, the formalism can be applied exactly only to the case of atomic hydrogen. Hydrogen-like treatments form the basis of all photoionization calculations in the x-ray region. At lower energies a simple hydrogen-like treatment is inadequate and photoionization calculations require estimates of the wave functions of the atomic system both before and after ionization takes place which are accurate in the regions of electron configuration space relevant to the calculations.

Such wave functions are difficult to obtain. Hartree-Fock wave functions are available for the ground states of most atoms for  $Z < 36$ , and provide a moderately good approximation for photoionization calculations, although they neglect correlation effects which may be important. For excited states of atomic systems, Hartree-Fock calculations may be carried out, but at present this has only been done in a few cases.<sup>3</sup> Calculations of continuum states representing a system consisting of an ionic core plus an unbound electron have been done mainly with electron scattering in mind. Since the emphasis in such calculations is on the asymptotic form of the wave functions at large distances, they, in general, provide much poorer estimates in the regions of configuration space important for photoionization calculations than do Hartree-Fock calculations for the ground states of atoms.

<sup>1</sup> See H. Hall, Revs. Modern Phys. 8, 358 (1936), and H. Bethe and E. Salpeter, in *Encyclopedia of Physics*, edited by S. Flügge (Springer-Verlag, Berlin, 1956), Vol. 35, Sec. 69.

<sup>2</sup> A good recent review of low-energy photoionization calculations is not available. Most of the material through 1956 is contained in rather condensed form in the article by G. L. Weissler, *Encyclopedia of Physics*, edited by S. Flügge (Springer-Verlag, Berlin, 1956), Vol. 21, pp. 366-441. For reviews of earlier work, see D. R. Bates, Monthly Notices Roy. Astron. Soc. 106, 432 (1946), and M. J. Seaton, Proc. Roy. Soc. A208, 408, 418 (1951).

<sup>3</sup> See, for example, R. S. Knox, Phys. Rev. 110, 375 (1958).

Experimental work<sup>4</sup> on atomic photoionization at low energies has been confined mainly to the rare gases and the alkalis, primarily because these are the only elements that may be studied as free atoms. Work on the rare gases is difficult, since the region of spectral interest lies in the far ultraviolet. Experiments on the alkalis are hampered by the small magnitude ( $\sim 10^{-19}$  cm<sup>2</sup>) of the cross sections near threshold and by the difficulty of obtaining purely monatomic vapors. Owing to these practical difficulties, little experimental work has been done and, in addition, it has been limited to an extremely narrow range of energies (usually a few electron volts above threshold, never more than 10 or 20).

Since little information is available, a logical step towards a better understanding of low-energy photoionization is the calculation in an approximate but consistent fashion of cross sections for a number of atoms over a broad spectral range. We have performed such calculations for electrons in the outer subshells of the atoms Ne, Ar, Kr, Na, and He, and of the ions Cu<sup>+</sup> and Ag<sup>+</sup>. The spectral range covered was from the photoionization threshold to about 100 eV above it for all cases except Na and He. The study of the rare gases was extended below threshold by computing the oscillator strengths for a number of discrete transitions. The calculations were performed using a central-field model which, although simple, should predict the gross spectral shape of the cross sections. The calculations are exploratory in nature and are intended to complement our knowledge of low energy photoionization and thus to point the way towards better approximations.

The cross section for absorption of a beam of photons of energy  $h\nu$  greater than the first ionization potential of the atom is given by the dipole approximation formula<sup>5</sup>

$$\sigma(h\nu) = \frac{4\pi\alpha a_0^2}{3} h\nu \left| \int \psi_0(\mathbf{r}_1, \mathbf{r}_2, \dots, \mathbf{r}_N) \right. \\ \times \sum_i \mathbf{r}_i \psi_f(\mathbf{r}_1, \mathbf{r}_2, \dots, \mathbf{r}_N) d\tau \left. \right|^2. \quad (1)$$

<sup>4</sup> See Hall, reference 1.

<sup>5</sup> See Bethe and Salpeter, reference 1, Secs. 59 and 69.

In (1),  $\psi_0$  and  $\psi_f$  are the wave functions of a single atom before and after absorption expressed in terms of the electron coordinates  $\mathbf{r}_i$ . The wave functions are expressed in atomic units, the integration is over the entire electron configuration space and the sum is over all atomic electrons.  $\psi_0$  is normalized to unit amplitude and  $\psi_f$  per unit energy range; i.e.,

$$\int |\psi_0|^2 d\tau = 1, \quad \int \psi_f(E) \psi_f(E') d\tau = \delta(E - E'),$$

where  $E$  is the total energy of  $\psi_f$ ,  $\alpha$  is the fine structure constant ( $1/137$ ). The atomic radius  $a_0$  ( $a_0 = 5.29 \times 10^{-9}$  cm) appears in (1) since  $\mathbf{r}_i$  is expressed in atomic units and  $\sigma$  in  $\text{cm}^2$ .

Equation (1) is valid for energies  $h\nu \ll mc^2$ . When single ionization takes place,  $\psi_f$  must represent the system consisting of an ion plus a free electron of energy  $\epsilon$ . In the present treatment we shall ignore multiple ionization corresponding to the emission of two or more electrons.

If  $I$  is the first ionization potential of the atom the photon energy  $h\nu$  and electron energy  $\epsilon$  obey the Einstein relation

$$h\nu = I + \epsilon.$$

This relation assumes that the ion is left in its ground state. For low photon energies the relation is exactly true but not for low electron energies, since for a given electron energy the ion may, in general, be left in an infinity of excited states, each corresponding to a different value of  $h\nu$ . In what follows we adopt the electron energy  $\epsilon$  as our independent variable.

The numerical evaluation of (1) requires estimates of  $\psi_0$  and  $\psi_f$ . To obtain these we make the following assumptions:

(a)  $\psi_0$  and  $\psi_f$  are antisymmetrized products of one-electron wave functions.  $\psi_0$  and  $\psi_f$  are each approximated by a single Slater determinant.

(b) Of the  $N$  one-electron wave functions from which  $\psi_0$  and  $\psi_f$  are formed,  $N-1$  are exactly the same for initial and final states. Under these assumptions,<sup>6</sup> the integral in (1) reduces to an integral over one-electron wave functions,

$$M = \int \phi_0(\mathbf{r}_1) \mathbf{r}_1 \phi_f(\mathbf{r}_1) d\tau_1. \quad (2)$$

In order to proceed further, the one-electron wave functions  $\phi_0(\mathbf{r}_1)$  and  $\phi_f(\mathbf{r}_1)$  must be estimated. These functions should describe as accurately as possible the spatial distribution of a single electron before and after photon absorption.

<sup>6</sup> It is also assumed that the one-electron wave functions are separable in radial and angular coordinates (spin is ignored in our treatment) and that the cross section is averaged over the orientation of the axis of quantization. Under these assumptions (2) reduces to integrals involving the radial functions only. See, for example, Bates, reference 2.

Assumption (a) is the starting point of the central-field description of atomic structure. Minimizing the total energy of an antisymmetrized product leads, as is well known,<sup>7</sup> to the Hartree-Fock equations, which may be solved numerically for the individual one-electron wave functions. Such one-electron wave functions provide, for all except the lightest atoms, the best spatial representation of the electrons in the outer subshell of an atom in its ground state presently available and have been used in most of the low-energy photoionization calculations performed to date, including the present work.

The choice of realistic final-state one-electron wave functions requires some discussion. First of all, it should be pointed out that in most of the previous work of low-energy photoionization assumption (b) is not made. The usual approach<sup>8</sup> is to assume final-state wave functions which are antisymmetrized products of a free-electron wave function and the one-electron wave functions of the ionic core. Under the assumption that the core functions are known (and, of course, they can be obtained by a solution of the Hartree-Fock equations for the ground state of the ion) and that the total wave function satisfies the Schrödinger equation, the radial part of the free one-electron wave function satisfies an inhomogeneous integro-differential equation analogous to the Hartree-Fock equation for an electron bound in a particular subshell of an atom. The resulting equation can be interpreted physically as describing an electron moving in the effective central field of the residual ion with allowance made for electron exchange by the inhomogeneous terms of the equation. Under these assumptions the integral in (1) reduces to the product of an integral over one electron functions of the form of (2) and an "overlap" integral which describes the relaxation of the ionic core.

Assumption (b) implies that the ionic core is unrelaxed. The assumption leads to the interpretation of the one-electron orbital energies for the various electron orbitals of an atom as ionization potentials for the electrons in the respective subshells.<sup>9</sup>

While the one-electron orbital energies generally are somewhat larger than the respective ionization potentials<sup>10</sup> the difference is never more than 15–20% for the outer subshells, which implies that (b) is a moderately good approximation. In the present work we make one further assumption, namely,

(c) The one-electron free wave functions are eigenfunctions of the same effective central potential as the ground-state functions  $\phi_0(\mathbf{r}_1)$ .

Physically (c) means we describe the electron being ionized as moving in the same effective central field

<sup>7</sup> D. R. Hartree, *The Calculation of Atomic Structures* (John Wiley & Sons, Inc., New York, 1957).

<sup>8</sup> See Seaton, reference 2, for an outline of this approach. Also M. J. Seaton, Trans. Roy. Soc. (London) A245, 58 (1953).

<sup>9</sup> T. Koopmans, Physica 1, 104 (1933).

<sup>10</sup> J. C. Slater, Phys. Rev. 98, 1039 (1955).

both before and after ionization takes place.<sup>11</sup> This treatment explicitly ignores the effects of electron exchange in the computation of continuum state wave functions. However, exchange effects are to some extent contained implicitly, since the effective central potential of the ground state contains a contribution due to electron exchange.

Assumptions (b) and (c) would appear to be more unrealistic than the Hartree-Fock-like treatment of reference 9. However, our approach has much to recommend it, particularly since we are interested in the spectral shape of the cross sections over a rather large energy range. First, the "best" effective central field from the standpoint of photoionization calculations is neither the field of the relaxed ion nor the field of the unrelaxed ionic core which we use, but something between these two extremes. The use of a relaxed core assumes no effect<sup>12</sup> (apart from exchange) of the outgoing electron on the ionic field while the use of an unrelaxed core overestimates this effect. Near the edge of the atom the effect is small and the ionic field is a good approximation. However, closer to the nucleus the effective central field is probably more like the unrelaxed ionic field. While the difference between the two fields is small, one would expect the relaxed field to provide good results for those calculations in which the important regions of electron configuration space are near the edge of the atom. This is just the region that is important for low-energy calculations (where exchange effects are also large); i.e., in the range from threshold to about 10 to 20 eV above it. At higher energies the unrelaxed field is probably the better approximation.

Second, the use of an unrelaxed core and the neglect of exchange means that the initial and final one-electron wave functions are eigenfunctions of the same central potential Hamiltonian. The use of a one-electron central potential model for the photoionization means that the dipole length, velocity, and acceleration forms for the matrix-element integrals, which are the same when exact many-electron eigenstates are used, are also the same in our approximation. A central potential model has the added advantage, as we will see, that one-electron sum rules apply to the photoionization from the various subshells of the atom.

Finally, the use of a relaxed ionic core implies that the ion is left in its ground-state configuration; i.e.,

<sup>11</sup> It should be emphasized that this approach is not new. Hargreaves [Proc. Cambridge Phil. Soc. **25**, 75 (1929)] performed calculations of this type for Li. Apparently the poor agreement of Hargreaves' results with experimental evidence discouraged further calculations of this kind. [See B. Trumpy, Z. Physik **71**, 720 (1931)]. It should be noted, however, that more recent calculations give no better agreement with experiment than those of Hargreaves [see, for example, A. Burgess and M. Seaton, Monthly Notices Roy. Astron. Soc. **120**, 119 (1960), especially Fig. 4 and the references quoted therein].

<sup>12</sup> Attempts to correct for this effect and produce a more realistic central potential for the case of scattering of electrons by atoms have recently been made. See M. H. Mittleman and K. M. Watson, Phys. Rev. **113**, 198 (1959).

that  $h\nu = I + \epsilon$ . While this is exactly true<sup>13</sup> for  $h\nu$  below the energy of the first excited state of the ion and is an excellent approximation at all energies, multiply excited states may have some effect at moderately high energies, although the total contribution to the cross section for any given electron energy is probably less than 10%. Bethe<sup>14</sup> has shown that when product wave functions are used, the average energy of the ionic core is the same after ionization as before, regardless of its final state of excitation. This result means that calculations based on the assumption of an unrelaxed core may be viewed in a broader sense; i.e., that they describe on the average the photoionization which produces an electron of energy  $\epsilon$  regardless of the frequency of light causing the process and the resulting energy of the ionic core.

As mentioned earlier, in the present work we adopt the electron energy  $\epsilon$  as our independent variable. Multiple excitation will tend to "smear out" rapid variations in the energy dependence of the photoionization cross section. A similar "smearing" is to be expected due to the effects of electron correlation which will be particularly important at low electron energies near the photoionization threshold. These correlation effects are not treated in the present paper.

## II. METHOD OF CALCULATION

### A. The Central Potential

The radial Hartree-Fock equation for an electron in the  $n$ th subshell of an atom (or ion) may be written as

$$\left[ \frac{d^2}{dr^2} + G_{nl}(r) + \epsilon_{nl} - \frac{l(l+1)}{r^2} \right] P_{nl} = X_{nl}(r). \quad (3)$$

Here  $P_{nl}(r)$  is the Hartree-Fock radial bound-state orbital,  $\epsilon_{nl}$  is the orbital energy (in rydbergs), and  $G_{nl}(r)$  and  $X_{nl}(r)$  are the potential and exchange terms.<sup>15</sup> In (3),  $r$  is expressed in atomic units and  $P_{nl}(r)$  is assumed normalized so that  $\int_0^\infty P_{nl}^2(r) dr = 1$ .

The simplicity of the form of (3) is somewhat misleading since  $G_{nl}(r)$  and  $X_{nl}(r)$  are functions which depend on integrals involving all of the other  $nl$  orbitals in the atom. (3) is thus one of a set of coupled integro-differential equations which must be solved simultaneously, there being as many equations as there are filled (or partially filled) subshells in the atom. An iterative solution of this coupled set of equations by numerical methods yields bound-state orbitals  $P_{nl}(r)$  and orbital energies  $\epsilon_{nl}$  for each subshell.

<sup>13</sup> The range of exact validity varies from atom to atom. For argon it is true for  $h\nu < 32$  eV, for Na for  $h\nu < 50$  eV.

<sup>14</sup> H. A. Bethe (private communication). The result is rigorously true only if exchange is neglected. The use of the unrelaxed core approximation has been stressed by Professor Bethe. Communications with Professor Bethe provided the starting point of the work described here. I would like to thank Professor Bethe for his advice and encouragement.

<sup>15</sup> The detailed form of  $G_{nl}(r)$  and  $X_{nl}(r)$  may be found in reference 7, Chaps. 3 and 6.

We define a central potential  $V_{nl}(r)$  for the  $nl$ th subshell in terms of the radial orbital  $P_{nl}(r)$  and energy  $\epsilon_{nl}$  by means of the radial Schrödinger equation:

$$\left( \frac{d^2}{dr^2} + V_{nl}(r) + \epsilon_{nl} - \frac{l(l+1)}{r^2} \right) P_{nl}(r) = 0. \quad (4)$$

From (3) and (4)

$$V_{nl}(r) = G_{nl}(r) - X_{nl}(r)/P_{nl}(r). \quad (5)$$

While the evaluation of  $V_{nl}(r)$  from a previously determined solution of the Hartree-Fock equations<sup>16</sup> (3) is straightforward, it leads to numerical difficulties. First, the way of defining  $V_{nl}(r)$  leads to singularities at the nodes (if any) of  $P_{nl}(r)$ . Second,  $V_{nl}(r)$  must approach  $2Z/r$  as  $r \rightarrow 0$  and  $2z/r$  as  $r \rightarrow \infty$  where  $Z$  is the nuclear charge and  $z$  the ionic charge ( $z=1$  for neutral atoms). While the form of (5) assures the proper asymptotic forms [ $G_{nl}(r) \rightarrow 2Z/r$  as  $r \rightarrow 0$ ;  $G_{nl}(r) \rightarrow 2z/r$  as  $r \rightarrow \infty$ ; and  $X_{nl}(r)$  vanishes faster than  $P_{nl}(r)$  as  $r \rightarrow 0$  and  $r \rightarrow \infty$ ] tabulated solutions of (3) are only given to two or three significant figures at large distances. We found that this accuracy was insufficient to determine an effective potential from (4) directly, given  $P_{nl}(r)$  and  $\epsilon_{nl}$ .<sup>17</sup> The procedure we adopted for determining  $V_{nl}(r)$  was to evaluate directly the functions  $G_{nl}(r)$  and  $X_{nl}(r)$  from the radial wave functions for each subshell. Although this method assures the correct asymptotic behavior of  $V_{nl}(r)$ , it still leaves the function singular at nodes of  $P_{nl}(r)$ . We have smoothed through these singularities in each case. Re-evaluation of  $P_{nl}(r)$  and  $\epsilon_{nl}$  using (4) has shown that the errors introduced by the smoothing are small.

### B. Solution of the Radial Equation for Continuum States

Continuum state radial wave functions  $P_{\epsilon l}(r)$  for positive electron energy  $\epsilon$  have been obtained by solving (4) with  $P_{nl}(r)$  replaced by  $P_{\epsilon l}(r)$  and  $\epsilon_{nl}$  replaced by  $\epsilon$ . Although the numerical solution of (4) is straightforward, several aspects of our method deserve mention.

Since the energy range we wished to cover was large (0 to about 10 rydbergs) and the potential  $V_{nl}(r)$  varies rapidly "within the atom," we adopted the Runge-Kutta method of solution<sup>18</sup> with the mesh of

<sup>16</sup> The Hartree-Fock solutions used were the following: Ne, B. Worsley, Can. J. Phys. **36**, 298 (1958); Ar, D. R. Hartree, Proc. Roy. Soc. (London) **A166**, 450 (1938); Kr and Ag<sup>+</sup>, B. Worsley, *ibid.* **A247**, 390 (1958); Na, D. R. Hartree and W. Hartree, *ibid.* **A193**, 299 (1948); He, W. Wilson and R. Lindsay, Phys. Rev. **47**, 681 (1935); Cu<sup>+</sup>, D. R. Hartree and W. Hartree, Proc. Roy. Soc. (London) **A151**, 490 (1936).

<sup>17</sup> We tried to do this both by direct evaluation of  $P_{nl}(r)$  from the equation using numerical differentiation and by using the analytic forms for  $P_{nl}(r)$  given by P. Lowdin and K. Appel [Phys. Rev. **103**, 1746 (1956)]. Neither procedure was satisfactory.

<sup>18</sup> The Runge-Kutta method specifies the solution of an equation such as (4) at a point  $r_0+h$  given the solution at the point  $r_0$ . See, e.g., J. B. Scarborough, *Numerical Analysis* (John Hopkins University Press, Baltimore, Maryland, 1950), p. 301. All of the computations referred to in this paper were done by machine computation (704 Fortran).

integration specified arbitrarily. The use of an arbitrary mesh in calculations of this type where the functions may vary rapidly in certain regions of integration has decided advantages over the techniques of transforming the basic equation (4) to fit a given set of circumstances or of simply doubling or tripling a given size mesh as is generally done in hand computation.

The integration of (4) was started in each case at  $r=0$  using the power series expansions given by Hartree.<sup>19</sup> The normalization of the wave functions at large distances should be

$$P_{\epsilon l}(r) \rightarrow \pi^{-\frac{1}{2}} \epsilon^{-\frac{1}{2}} \sin[\epsilon^{\frac{1}{2}} r - l\pi/2 - z\epsilon^{-\frac{1}{2}} \ln 2\epsilon^{\frac{1}{2}} r + \delta_l], \quad (6)$$

where  $\delta_l$  is a constant phase shift.

The normalization of solutions can be effected in many ways, the usual approach<sup>20</sup> being to express  $P_{\epsilon l}(r)$  in terms of the regular and irregular Coulomb wave functions  $F_l(\epsilon^{\frac{1}{2}} r)$  and  $G_l(\epsilon^{\frac{1}{2}} r)$ . For numerical work a more convenient procedure is available<sup>21</sup> which is easily adapted to machine calculation. The method, as applied in the present work, is presented in some detail in Appendix A for reference purposes.

### C. Radial Matrix Elements and Photoionization Cross Sections

Under our assumption of a central potential model the photoionization cross section  $\sigma_{nl}(\epsilon)$  for the  $nl$ th subshell of an atom reduces to

$$\sigma_{nl}(\epsilon) = (4\pi\alpha a_0^2/3)(\epsilon - \epsilon_{nl})(C_{l-1}R_{l-1}^2 + C_{l+1}R_{l+1}^2). \quad (7)$$

In the above,  $-\epsilon_{nl}$ , the binding energy for an electron in the  $nl$ th subshell, is assumed equal to the ionization potential for that subshell. The numerical factors  $C_{l\pm 1}$  arise from averaging over all initial states of angular momentum quantum number  $m$  and summing over all final states.<sup>22</sup> The factors  $R_{l\pm 1}$  are the radial dipole length matrix elements

$$R_{l\pm 1} = \int_0^\infty P_{nl}(r) r P_{\epsilon, l\pm 1}(r) dr, \quad (8)$$

where  $P_{nl}(r)$  and  $P_{\epsilon, l\pm 1}(r)$  are the bound and continuum radial wave functions defined in Sec. B. Alternative expressions for  $R_{l\pm 1}$  are the dipole velocity form,

$$R_{l\pm 1} = \frac{2}{\epsilon - \epsilon_{nl}} \int_0^\infty P_{nl}(r) \times \left[ \frac{2l+1\pm 1}{2r} P_{\epsilon, l\pm 1}(r) \pm \frac{d}{dr} P_{\epsilon, l\pm 1}(r) \right] dr, \quad (9)$$

<sup>19</sup> See reference 7, p. 81.

<sup>20</sup> See, for example, reference 11.

<sup>21</sup> D. R. Bates and M. J. Seaton, Monthly Notices Roy. Astron. Soc. **109**, 698 (1949). Also M. J. Seaton and G. Peach, Proc. Phys. Soc. (London) **79**, 1296 (1962).

<sup>22</sup> See Bates, reference 2.

TABLE I. Photoionization cross sections computed using length ( $L$ ), velocity ( $V$ ), and acceleration ( $A$ ) formulas for  $\text{Ag}^+$  and  $\text{Cu}^+$ .

$\epsilon$ (Ry)	$L$	$\sigma \times 10^{18}$ (cm $^2$ )			$\text{Cu}^+$		
		$\text{Ag}^+$	$V$	$A$	$L$	$V$	$A$
0.0	21.0	18.1	13.1	8.33	8.23	7.53	
1.0	30.0	24.2	15.7	12.28	12.14	11.88	
2.0	31.2	25.3	23.2	11.92	11.92	11.81	
4.0	13.6	9.2	7.6	9.63	9.48	9.46	
6.0	3.4	2.1	2.1	7.06	7.06	7.07	

and the dipole acceleration form,

$$R_{l\pm 1} = \frac{4}{(\epsilon - \epsilon_{nl})^2} \int_0^\infty P_{nl}(r) \frac{dV_{nl}(r)}{dr} P_{\epsilon, l\pm 1}(r) dr. \quad (10)$$

The expressions (8), (9), and (10) are exactly equal if  $P_{nl}(r)$  and  $P_{\epsilon, l\pm 1}(r)$  are eigenfunctions and  $\epsilon_{nl}$  and  $\epsilon$  are the corresponding eigenvalues of the same central potential. From a numerical standpoint (8) is preferable since, if wave functions are known numerically,  $R_{l\pm 1}$  can be evaluated by direct integration whereas (9) and (10) require differentiation of the free wave function and the central potential, respectively. In practice it was relatively easy to evaluate all three forms<sup>23</sup> since the derivative of the radial wave function is computed at the same time as the wave function by the Runge-Kutta procedure and the derivative of the potential can be obtained by numerical differentiation.

#### D. Accuracy of the Calculations

The numerical accuracy of our work can be gauged by a comparison of cross sections computed using the length, velocity, and acceleration forms of the matrix elements given by (8), (9), and (10). For all of the cases considered the spectral shape of the cross section is the same regardless of which form is used. The three formulas give results accurate to better than 10% for all of the calculations involving nodeless shells (He, Ne, Cu $^+$ ) and for the calculations for argon. For the Kr and Ag $^+$  calculations the accuracy is poorer, partly due to the smoothing over the singularities previously mentioned, but mostly due to inaccuracies in determining the exchange potential  $X_{nl}(r)$ .<sup>24</sup> The accuracy of the sodium calculations is also less than 10% since the cross section is small owing to cancellation of positive and negative portions of the integrands in formulas (8), (9), and (10). In Table I we list the cross sections obtained for one of the better cases (Cu $^+$ ) and one of the poorer cases (Ag $^+$ ) by way of illustration. Better accuracy could, of course, be obtained by more careful calculations.

<sup>23</sup> A fourth form, obtained by differentiating (9) by parts, which expresses  $R_{l\pm 1}$  in terms of the free wave function and the bound-state functions and its first derivative was also evaluated.

<sup>24</sup>  $G_{nl}(r)$  and  $X_{nl}(r)$  were evaluated by direct Simpson's rule integration of the Slater integrals involved. This procedure leads to round-off errors for atoms of large  $Z$ .

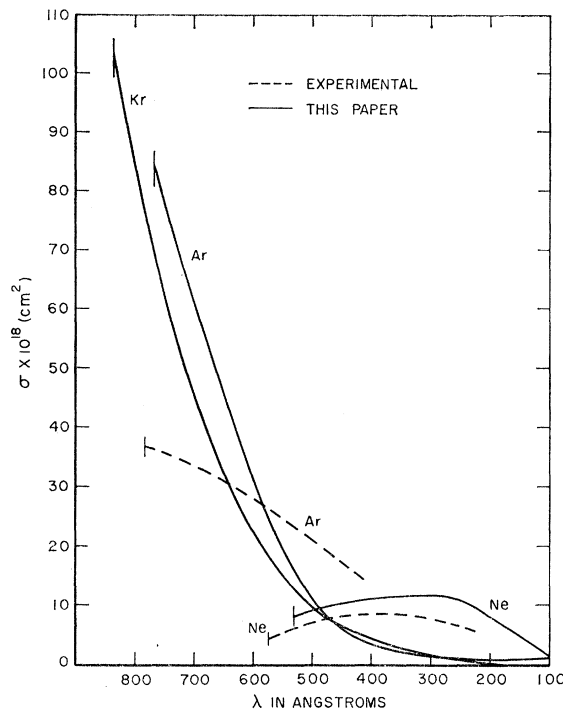


FIG. 1. Photoionization cross sections for Ne, Ar, and Kr.

### III. PHOTOIONIZATION RESULTS

#### Ne, Ar, Kr, Na, He, Ag $^+$ , Cu $^+$

The results of the photoionization calculations for Ne, Ar, and Kr are plotted in Fig. 1 along with available experimental evidence on Ne and Ar.<sup>25</sup> Since our calculations refer only to ionization of outer subshell electrons, the figure does not show the peaks due to  $2s \rightarrow e\bar{p}$  and  $3s \rightarrow e\bar{p}$  transitions in Ne and Ar which are observed experimentally. The curves are plotted against  $\lambda = 911.2/(\epsilon - \epsilon_{nl})$  (Angstroms). Although our chief purpose here is not comparison with experimental results, Fig. 1 does show that our model gives correct order of magnitude estimates. The spectral shape for

TABLE II. One electron energies ( $-\epsilon_{nl}$ ) and ionization potentials ( $I$ ) for all cases treated.

Element	Configuration	$-\epsilon_{nl}$ (Ry)	$I$ (Ry)
Ne	(2p) $_6$	1.705	1.585
Ar	(3p) $_6$	1.181	1.158
Kr	(4p) $_6$	1.06	1.029
Cu $^+$	(3d) $^{10}$	1.613	1.491
Ag $^+$	(4d) $^{10}$	1.69	1.579
Na	3s	0.361	0.3777
He	(1s) $_2$	1.836	1.807

<sup>25</sup> Ne, R. W. Ditchburn, Proc. Phil. Soc. London A76, 233 (1960); Ar, Po Lee and G. L. Weissler, Phys. Rev. 99, 540 (1955). Kr has also been studied experimentally; see A. Pery-Thorne and W. R. S. Garton, Proc. Phys. Soc. (London) A76, 833 (1960). Seaton has calculated the cross section for Ne (Seaton, reference 2). His results have the same spectral shape as ours and lie closer in magnitude to the experimental values.

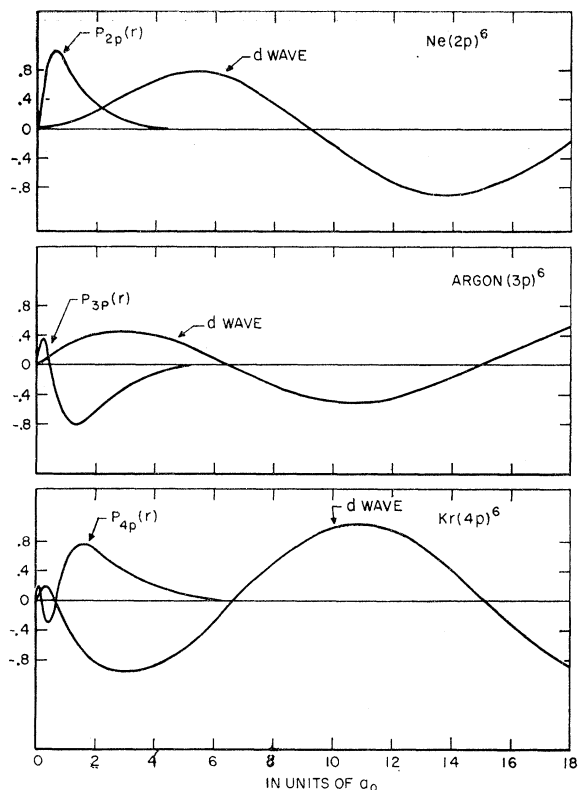


FIG. 2. Outer subshell radial wave functions and  $d$  waves for  $\epsilon=0$  for Ne, Ar, and Kr.

neon is similar to that observed even though the orbital binding energy<sup>26</sup> (1.705 Ry) is 7% higher than the observed ionization potential (1.585 Ry). (See Table II). The observed drop of the cross section for Ar near threshold is reproduced by the calculation although the calculated curve is much steeper. As mentioned in Sec. I, correlation effects which we have not considered are expected to smear out this rapid drop.

The spectral shape of the cross sections can be understood by considering the energy dependence of the dipole matrix integral (Eq. 8). In Fig. 2 we have plotted the ground-state radial function  $P_{nl}(r)$  and the  $d$  wave for zero energy [i.e.,  $P_{el}(r)$  for  $\epsilon=0$ ,  $l=2$ ] for Ne, Ar, and Kr. The  $d$ -wave matrix element is several times larger than the  $s$ -wave matrix element for Ne, Ar, and Kr at all energies and its spectral behavior will determine the spectral behavior of the cross section. From Fig. 2 we see that the  $d$ -wave matrix element will be small and positive for Ne but large and negative for Ar and Kr at  $\epsilon=0$ . As the electron energy increases, the  $d$  waves in each case will "move in" towards the origin. For Ne this will cause an increase in cross section at first and then eventually a decrease when the first node of the  $d$  wave has moved close enough to the origin for negative contributions to the integrand to become

<sup>26</sup>The orbital binding energies and experimental ionization potentials for all cases treated are listed in Table II.

important. In the range of energies considered (0 to 10 Ry) the  $d$ -wave matrix element is positive. Since it must be positive in the high-energy limit, any reversal of sign of the matrix element at higher energies is unlikely. For Ar and Kr, on the other hand, the matrix element is negative at  $\epsilon=0$  and will decrease in magnitude as the energy increases, becoming zero when positive and negative portions of the integrand are equal. This occurs at about  $\epsilon=2$  for Ar at about  $\epsilon=2.4$  for Kr. At higher energies the matrix element is positive. As in the case of neon, further sign reversals are unlikely at higher energies. The  $d$ -wave matrix elements for Ne, Ar, and Kr are shown in Fig. 3.

For sodium, almost complete cancellation of the positive and the negative portions of the integrands in Eq. (8) occurs at threshold. In Fig. 4 we show the cross sections calculated using our model along with the earlier calculations of Seaton<sup>21</sup> using the relaxed core approximation and a recent experimental determination.<sup>27</sup> The spectral shape of all three curves is the same. Our calculations predict the minimum in the curve too close to threshold, partially due to the fact that  $\epsilon_{3s}$  is less than the ionization potential for Na ( $\epsilon_{3s}=0.361$ ,  $I_{\text{Na}}=0.3777$ ), and the agreement with experiment is poorer than for Seaton's calculations. Nevertheless, the model does predict the gross features (magnitude and spectral shape) of the cross section.

Helium is the only atom besides hydrogen whose photoionization cross section has been studied extensively.<sup>28</sup> Agreement between theory and experiment in the region between threshold and about 2 Ry above it is excellent (10–20%) compared to the results for heavier atoms. Calculations have been made at higher energies also, mainly because of their importance in estimating the Lamb shift correction to the helium ground-state energy.

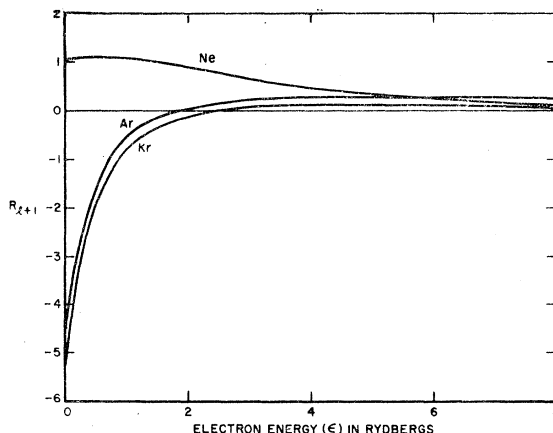


FIG. 3. Matrix elements for  $p \rightarrow d$  transitions in Ne, Ar, and Kr.

<sup>27</sup>R. D. Hudson, Bull. Am. Phys. Soc. **5**, 496 (1960).

<sup>28</sup>See A. Dalgarno and A. L. Stewart Proc. Phys. Soc. (London), **A76**, 49 (1960) for a discussion of work prior to 1960.

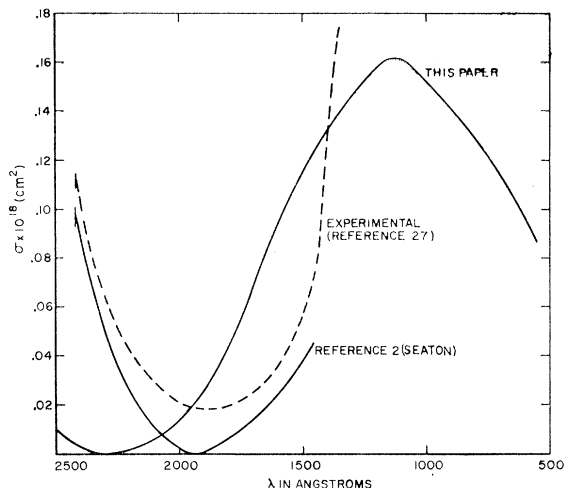


FIG. 4. Photoionization cross sections for Na. Note expanded scale.

We have calculated the helium cross section in the range 0 to 100 Ry mainly for comparison with other calculations and experiments. The results for the range 0–2 Ry are shown in Fig. 5 along with a recent measurement<sup>29</sup> and the “best” values derived from an analysis of experimental data and calculations by Stewart and Wilkinson.<sup>30</sup>

Salpeter and Zaidi<sup>31</sup> have recently computed the photoionization cross section for He in the region from threshold to 1000 Ry. In their calculations they used the dipole velocity form of the matrix element and an 18 parameter variational wave function for the He ground state. Their continuum state wave functions were computed using the effective potential of the  $\text{He}^+$  ion (relaxed core approximation) with exchange neglected. Their results at threshold are about 50% higher than the results of calculations and experiments. This discrepancy, which according to the authors is due to the use of a more accurate ground-state wave function than other calculations, is hard to understand. However, at higher energies (10–1000 Ry) their method should give realistic results. In Table III we give a comparison of cross sections computed at a few energies by our

method with those of Salpeter and Zaidi. Length, velocity, and acceleration forms are given to indicate the numerical accuracy. The agreement is excellent.

The spectral shape of the Na and He cross sections can be understood in terms of the energy dependence of the  $s-p$  dipole matrix element. For He this matrix element is always positive as was the case for Ne and consequently the cross section decreases monotonically. For Na, on the other hand, the matrix element is negative at threshold and goes through zero at low energy. Consequently, the cross section goes through zero and then rises, finally falling off again at higher energies as shown in Fig. 4.

The results for the rare gases and Na lead to the generalization that the photoionization cross sections from atomic subshells whose radial wave functions are nodeless have, in general, a different spectral shape than those from subshells whose radial wave functions have nodes.<sup>32</sup> One would thus expect the cross sections from the subshells of the type  $(1s)^n$ ,  $(2p)^n$ ,  $(3d)^n$ , etc., to belong to the first category while all others belong to the second. To check this generalization we have calculated the photoionization from the closed subshells of  $\text{Cu}^+$ ,  $(3d)^{10}$  and  $\text{Ag}^+$ ,  $(4d)^{10}$ . The results are shown in Fig. 6. In accordance with our generalization the  $\text{Ag}^+$  cross section goes through a minimum at about 8 Ry above threshold due to the vanishing of the matrix element for

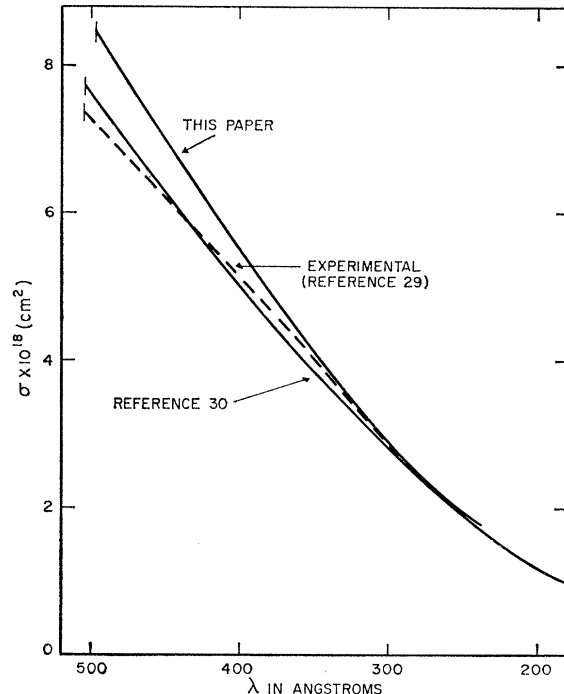


FIG. 5. Photoionization cross sections for He.

TABLE III. Photoionization cross sections for He.

$\epsilon$ (Ry)	$L$	$V$	$A$	$\sigma \times 10^{18} (\text{cm}^2)$ <sup>a</sup>
3.98107	0.617	0.615	0.612	0.603
10	0.0913	0.0913	0.0906	0.0943
50.1185	0.00115	0.00113	0.00111	0.00110
100	0.00012	0.00014	0.00013	0.000126

<sup>a</sup> This paper.

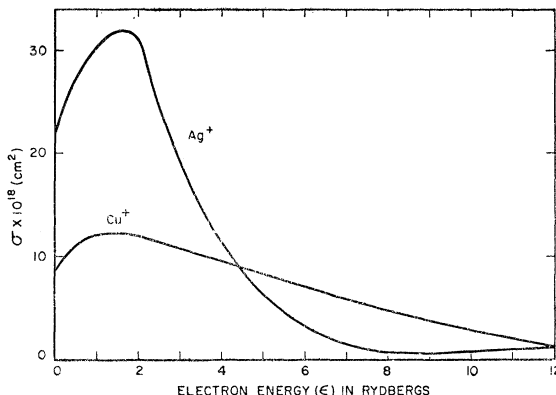
<sup>b</sup> See reference 31.

<sup>29</sup> D. J. Baker, Jr., D. E. Bedo and D. H. Tomboulian, Phys. Rev. **124**, 1471 (1961).

<sup>30</sup> A. L. Stewart and W. J. Wilkinson, Proc. Phys. Soc. (London) **A75**, 796 (1960).

<sup>31</sup> E. Salpeter and M. H. Zaidi, Phys. Rev. **125**, 248 (1962).

<sup>32</sup> This generalization has been reported previously. See abstracts by J. W. Cooper and by U. Fano, *Proceedings of the Second International Conference on the Physics of Electronic and Atomic Collisions, Boulder, Colorado, June, 1961* (W. A. Benjamin Inc., New York, 1961), pp. 7–10.

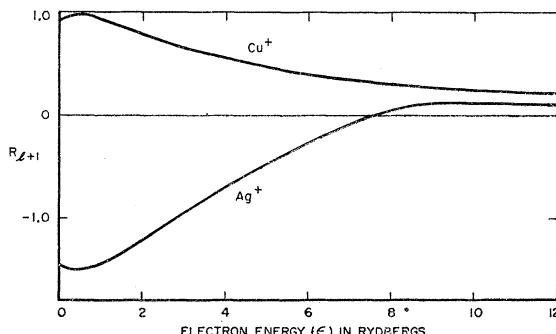
FIG. 6. Photoionization cross sections for  $\text{Ag}^+$  and  $\text{Cu}^+$ .

the  $d-f$  transition which dominates the spectral behavior of the cross section. For  $\text{Cu}^+$  on the other hand, the  $d-f$  matrix element is always positive and slowly varying, as was the case for He and Ne. The spectral dependence of these matrix elements is shown in Fig. 7.

The agreement of our calculations with experiments and other calculations in the low-energy region is somewhat better than one might expect for such a simple model. The main reason for this is that our use of the unrelaxed ionic core approximation compensates, to a certain extent, for the neglect of polarization effects while our use of an effective potential which includes the effects of exchange in the ground state to a certain extent compensates for our neglect of exchange in computing continuum states. However, the most important result of these calculations is not that they provide a method for computing cross sections to a fair degree of accuracy in a given spectral range, but that they give a reasonable estimate of the spectral shape of the cross section over a broad spectral range.

#### IV. RESULTS FOR DISCRETE TRANSITIONS

In a central field model<sup>33</sup> the oscillator strength for a single-electron transition between states of quantum

FIG. 7. Matrix elements for  $d-f$  transitions in  $\text{Ag}^+$  and  $\text{Cu}^+$ .

<sup>33</sup> See Bethe and Salpeter, reference 1, Sec. 61.

numbers  $nl$  and  $n'l'$  where  $l'=l\pm 1$  is

$$f_{nl \rightarrow n'l'} = -\frac{\tilde{l}}{3(2l+1)}(\epsilon_{n'l'} - \epsilon_{nl})R_{nl \rightarrow n'l'}{}^2, \\ \tilde{l}=l \quad \text{for} \quad l'=l-1, \quad \tilde{l}=l+1 \quad \text{for} \quad l'=l+1, \quad (11)$$

where  $\epsilon_{nl}$  and  $\epsilon_{n'l'}$  are the energy eigenvalues of the states  $nl$  and  $n'l'$  and  $R_{nl \rightarrow n'l'}$  is the radial matrix element

$$R_{nl \rightarrow n'l'} = \int_0^\infty P_{nl}(r)rP_{n'l'}(r)dr. \quad (12)$$

The calculation of oscillator strengths using a central potential model can be done in much the same way as the photoionization calculations except that Eq. (4) must be solved as an eigenvalue problem for values of  $\epsilon_{n'l'}$  and the corresponding functions  $P_{n'l'}(r)$  for various one-electron excited states  $n'l'$ .

We have computed one-electron energy eigenvalues and eigenfunctions for the first few  $s$  and  $d$  states of Ne, Ar, and Kr using the same potential as was used for the photoionization calculations.<sup>34</sup> The results, along with statistically weighted term values<sup>35</sup> (for excited states) and inner shell ionization potentials<sup>36</sup>, are listed in Table IV. Also shown are quantum defects  $\sigma_{nl}$ , defined by the relation  $\epsilon_{nl} = -(n-\sigma_{nl})^{-2}$ . The close agreement of the averaged term values and our computed orbital energies and their respective quantum defects indicates that our model gives a fairly realistic description of the radial wave functions for the excited states of the atom.

The oscillator strengths for transitions of a single electron in the outer subshells of Ne, Ar, and Kr to other one-electron states are shown in Table V. Also shown are oscillator strengths for transitions excluded by the Pauli principle, such as  $2p-1s$ , which are necessary for the application of one-electron sum rules to the total oscillator strength spectral distribution. The table shows that a small fraction of the total oscillator strength distribution is due to discrete transitions. The spectral distributions for Ar and Kr are similar and the total strength for discrete transitions is much larger for Ar and Kr than for Ne.

The discrete oscillator strength distribution can be considered as an extension of the continuum oscillator strength distribution

$$\frac{df_{l\pm 1}(\epsilon)}{d\epsilon} = \frac{1}{3(2l+1)}(\epsilon - \epsilon_{nl})R_{l\pm 1}{}^2, \quad (13)$$

where  $R_{l\pm 1}{}^2$  is the bound-continuum matrix element

<sup>34</sup> These computations were carried out using computer codes developed at the Rand Corporation. I would like to thank Dr. R. Latter and Dr. W. Karzas and Mr. J. Babcock for permission to use these codes and for instruction in their operation.

<sup>35</sup> C. M. Sitterly, *Atomic Energy Levels*, National Bureau of Standards Circular No. 467 (U. S. Government Printing Office, Washington, D. C., 1948).

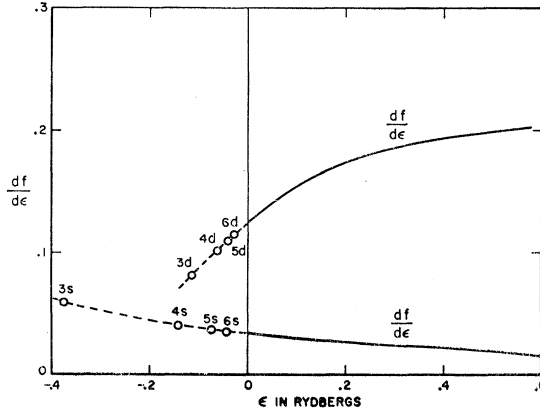
<sup>36</sup> K. Siegbahn, *Beta- and Gamma-Ray Spectroscopy* (North-Holland Publishing Company, Amsterdam, 1955).

TABLE IV. One-electron energies and quantum defects for Ne, Ar, and Kr.

$n'l'$	$-\epsilon_{n'l'}$	s states			$n'l'$	d states		
		$E(\text{exp})$	$\sigma_{n'l'}$	$\sigma(\text{exp})$		$E(\text{exp})$	$\sigma_{n'l'}$	$\sigma(\text{exp})$
$\langle \text{Ne} \rangle$								
1s	59.91	64.0	...	...	3d	0.1132	0.1121	-0.028
2s	3.364	3.56	...	...	4d	0.0637	0.0630	-0.039
3s	0.376	0.360	-1.37	-1.33	5d	0.0407	0.0403	-0.042
4s	0.141	0.139	-1.34	-1.32	6d	0.0282	0.0279	-0.044
5s	0.0744	0.0735	-1.33	-1.31	7d	0.0207	0.0205	-0.045
6s	0.0459	0.0456	-1.33	-1.32	8d	0.0158	0.0157	-0.045
7s	0.03110	0.0309	-1.33	-1.31				-0.019
$\langle \text{Ar} \rangle$								
1s	220.0	236.2			3d	0.1340	0.1274	-0.269
2s	21.47	24.2			4d	0.0744	0.0717	-0.334
3s	2.122	2.15			5d	0.0455	0.0452	-0.312
4s	0.319	0.304	-2.23	-2.19	6d	0.0311	0.0308	-0.330
5s	0.126	0.124	-2.18	-2.16				
6s	0.069	0.067	-2.19	-2.15				
$\langle \text{Kr} \rangle$								
1s	1024.6	1055.5			3d	7.9	7.1	
2s	137.0	142.0			4d	0.134	0.126	-1.27
3s	20.4	22.1			5d	0.0731	0.0731	-1.29
4s	2.01	2.00			6d	0.0446	0.0450	-1.27
5s	0.300	0.300	-3.18	-3.18	7d	0.0306	0.0308	-1.29
6s	0.122	0.121	-3.13	-3.13				-1.30
7s	0.067	0.066	-3.14	-3.11				

defined by Eq. (8). In order to make a direct comparison of the discrete spectral distribution of  $f$  as defined by Eq. (11) with the continuum distribution (13) the  $f$  values must be normalized per unit energy range by dividing by  $2(\epsilon_{n'l'} - \epsilon_{nl})^{\frac{1}{2}}$ .

Plots of  $df/d\epsilon$  and  $f_{nl \rightarrow n'l'}/2(\epsilon_{n'l'} - \epsilon_{nl})^{\frac{1}{2}}$  for the  $p \rightarrow s$  and  $p \rightarrow d$  transitions in Ne are shown on the same energy scale in Fig. 8. The discrete values for both series lie on the extrapolated continuum curve for all values of  $n$ . Similar plots are shown in Fig. 9 for  $p \rightarrow s$  transitions in Ar and Kr. For these transitions the discrete values show some scatter from the extrapolated continuum curve due to the inaccuracy of the numerical calculations. The scatterer is even greater for the case of  $p \rightarrow d$  transitions in Ar and Kr (not shown).

FIG. 8.  $df/d\epsilon$  and  $f_{nl \rightarrow n'l'}/2(\epsilon_{n'l'} - \epsilon_{nl})^{\frac{1}{2}}$  for  $p \rightarrow d$  and  $p \rightarrow s$  transitions in Ne.

## V. PROPERTIES OF THE OVER-ALL OSCILLATOR STRENGTH DISTRIBUTION—SUM RULES

For a one-electron central potential model the oscillator strength distributions for  $l'=l+1$  and  $l'=l-1$  transitions as defined by Eqs. (11) and (13) obey the following rules<sup>37</sup>:

$$\sum_{n'} \frac{f_{nl \rightarrow n'l'}}{\epsilon_{n'l'} - \epsilon_{nl}} = \frac{\tilde{l}}{3(2l+1)} \langle r^2 \rangle_{nl}, \quad (14)$$

TABLE V. One-electron oscillator strengths for Ne, Ar, and Kr.

Transition	$f_{nl \rightarrow n'l'}$	Transition	$f_{nl \rightarrow n'l'}$
$\langle \text{Ne} \rangle$			
2p-1s	-0.0531	2p-3d	0.0062
2p-2s	-0.1535	2p-4d	0.0033
2p-3s	0.0272	2p-5d	0.0018
2p-4s	0.0044	2p-6d	0.0011
2p-5s	0.0015		
2p-6s	0.0007		
$\langle \text{Ar} \rangle$			
3p-1s	-0.0056	3p-3d	0.196
3p-2s	-0.026	3p-4d	0.081
3p-3s	-0.242	3p-5d	0.043
3p-4s	0.055	3p-6d	0.022
3p-5s	0.0082		
3p-6s	0.0031		
$\langle \text{Kr} \rangle$			
4p-1s	-0.00104	4p-3d	-0.047
4p-2s	-0.0045	4p-4d	0.210
4p-3s	-0.0154	4p-5d	0.083
4p-4s	-0.294	4p-6d	0.046
4p-5s	0.0675	4p-7d	0.023
4p-6s	0.0108		
4p-7s	0.004		

<sup>37</sup> Bethe and Salpeter, reference 1, Secs. 61 and 62.

TABLE VI. One-electron expectation values for all cases treated.

	Ne	Ar	Kr	He	Na	$\text{Ag}^+$	$\text{Cu}^+$
$\langle r^2 \rangle_{nl}$	1.21	3.3	4.45	1.145	20.8	2.17	1.28
$\langle T \rangle_{nl}$	8.33	5.6	5.42	2.86	0.69	16.2	18.88
$[P_{nl}(r)/r]^2 _{r=0}$	$7.77 \times 10^2$	$2.6 \times 10^3$	$1.97 \times 10^4$	22.6	6.3	$1.2 \times 10^6$	$3.51 \times 10^4$

$$\sum_{n'} f_{nl \rightarrow n' l'} = -\frac{1}{3} \frac{l(2l-1)}{(2l+1)} \quad \text{for } l'=l-1 \\ = -\frac{1}{3} \frac{(l+1)(2l+3)}{2l+1} \quad \text{for } l'=l+1, \quad (15)$$

$$\sum_{n'} (\epsilon_{n' l'} - \epsilon_{nl}) f_{nl \rightarrow n' l'} = \frac{4\tilde{l}z}{3(2l+1)} \langle T \rangle_{nl} \quad (16)$$

$$\sum_{n'} (\epsilon_{n' l'} - \epsilon_{nl})^2 f_{nl \rightarrow n' l'} = \frac{4\tilde{l}z}{3(2l+1)} \left( \frac{P_{nl}(r)}{r} \right)^2 |_{r=0}. \quad (17)$$

In the above the sum over  $n'$  includes a summation over all discrete transitions defined by (11) and an integration over the continuum as defined by (13).  $\tilde{l}$  is defined in Eq. (11).  $\langle r^2 \rangle_{nl}$  and  $\langle T \rangle_{nl}$  are the  $nl$ -state expectation values of  $r^2$  and of the kinetic energy of an  $nl$ th subshell electron, respectively.  $P_{nl}(r)$  is the value of the  $nl$ th wave function defined by Eq. (3). Equations (14)–(17) express the  $m$ th moments ( $m=-1, 0, 1, 2$ ) of the spectral distribution  $f(\epsilon)$  in terms of expectation values of the  $nl$ th one electron state.<sup>38</sup> The expectation values  $\langle r^2 \rangle_{nl}$  and  $\langle T \rangle_{nl}$  may be computed from the wave function  $P_{nl}(r)$  by the formulas:

$$\langle r^2 \rangle_{nl} = \int_0^\infty P_{nl}^2 r^2 dr,$$

$$\langle T \rangle_{nl} = \int_0^\infty P_{nl}^2 V_{nl}(r) dr + \epsilon_{nl}.$$

In Table VI we list expectation values for all of the atomic subshells for which photoionization calculations were carried out.

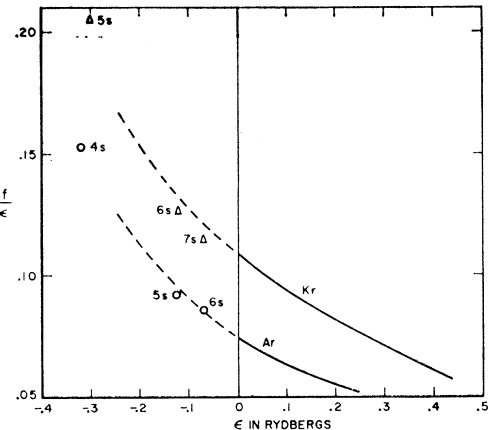
The expectation values can be used to predict the spectral shape of the oscillator strength distribution. In the present case, since we have computed the entire distribution (discrete and continuum) for the rare gases Ne, Ar, and Kr, we can get an idea of how much information can be obtained from the spectral moments by evaluating both sides of Eqs. (14)–(17). Since the distributions of Kr and Ar are similar we limit our discussion to Ne and Ar.

In Table VII we show a “balance sheet” for the  $p \rightarrow s$  transitions in Ne and Ar corresponding to Eqs.

(14)–(16). It was not practical to use Eq. (17) in the present work since the major contribution to the sum in this case is at electron energies greater than 10 Ry. In Table VII we also list the downward transitions such as  $2p-1s$  since these transitions, although excluded by the Pauli principle, must be included in a one-electron

TABLE VII. Contributions to Eqs. (14), (15), and (16) for Ne and Ar  $p \rightarrow s$  Transitions.

Transition	$(\epsilon_{n' l'} - \epsilon_{2p})$ (ry)	Eq. (14)	Eq. (15)	Eq. (16)
(Neon $p \rightarrow s$ transitions)				
$2p-1s$	-58216	0.0009	-0.053	3.091
$2p-2s$	-1.670	0.0912	-0.154	0.256
$2p-3s$	1.318	0.0207	0.027	0.036
$2p-4s$	1.553	0.0028	0.004	0.007
$2p-5s$	1.620	0.0009	0.002	0.002
$2p-6s$	1.648	0.0004	0.001	0.001
$2p-Es$	$1.708 - \infty$	0.0187	0.067	0.222
Totals		0.1356	-0.106	3.615
Totals computed from expectation values		0.1349	-0.111	3.702
(Argon $p \rightarrow s$ transitions)				
$3p-1s$	-218.80	0.0000	-0.006	1.225
$3p-2s$	-20.30	0.0013	-0.026	0.528
$3p-3s$	-0.953	0.2544	-0.242	0.231
$3p-4s$	0.851	0.0648	0.055	0.047
$3p-5s$	1.054	0.0078	0.008	0.009
$3p-6s$	1.100	0.0028	0.003	0.003
$3p-Es$	$1.181 - \infty$	0.0367	0.080	0.200
Totals		0.3678	-0.128	2.24
Totals computed from expectation values		0.3667	-0.111	2.48

FIG. 9.  $df/d\epsilon$  and  $f_{nl \rightarrow n' l'}/2(\epsilon_{nl} - \epsilon_{n' l'})^{1/2}$  for  $p \rightarrow s$  transitions in Ar and Kr.

<sup>38</sup> Equations may also be written for the moments corresponding to  $m=-2, -4$ , etc., and the moments may be evaluated from experimental data. However, these moments cannot be obtained directly from the  $nl$ th-state wave functions. Higher moments corresponding to  $m=3, 4$ , etc., are infinite.

TABLE VIII. Contributions to Eqs. (14), (15), and (16) for Ne and Ar  $p \rightarrow d$  transitions.

Transition	$\epsilon_{n'l'} - \epsilon_{2p}$ (ry)	Eq. (14)	Eq. (15)	Eq. (16)
Neon $p \rightarrow d$				
$2p-3d$	1.581	0.0038	0.0062	0.0097
$2p-4d$	1.630	0.0020	0.0033	0.0053
$2p-5d$	1.654	0.0012	0.0018	0.0030
$2p-6d$	1.666	0.0006	0.0011	0.0018
$2p-Ed$	$1.705 - \infty$	0.2667	0.94	4.94
Totals		0.2743	0.95	4.96
Totals computed from expectation values		0.2698	1.11	7.40
(Argon $p \rightarrow d$ )				
$3p-3d$	1.035	0.189	0.196	0.203
$3p-4d$	1.095	0.074	0.081	0.089
$3p-5d$	1.124	0.038	0.043	0.048
$3p-6d$	1.138	0.020	0.022	0.025
$3p-Ed$	$1.181 - \infty$	0.393	0.88	4.73
Totals		0.714	1.222	5.10
Totals computed from expectation values		0.733	1.111	4.98

treatment. The table shows that for  $p \rightarrow s$  transitions these excluded transitions make important contributions to the one-electron sums of Eqs. (14)–(16). Most of the “allowed” oscillator strength distribution for  $p \rightarrow s$  transitions is in the continuum. The sums in Eqs. (14)–(16) agree to the accuracy of our calculations with the sums computed directly from the expectation values.

For  $p \rightarrow d$  transitions in Ne and Ar there are no excluded transitions. Balance sheets for Eqs. (14)–(16) for  $p \rightarrow d$  transitions in Ne and Ar are shown in Table III. The table shows that practically all of the oscillator strength in Ne is in the continuum while for Ar about 70% of the distribution is due to continuum transitions.

The disagreement for  $p \rightarrow d$  transitions between totals computed directly by integration over the oscillator strength distribution and those obtained from expectation values in Table VIII is due to the fact that computations were only carried out to 10 Ry and the distribution extrapolated to higher energies. While the two values for Eq. (16) for Ne differ by about 30%, this is not surprising since slight changes in the extrapolation procedure will lead to large changes in the oscillator sum. This is shown in Fig. 10 where we have plotted  $df/d\epsilon$  and  $(\epsilon - \epsilon_{2p})df/d\epsilon$  for the  $p \rightarrow d$  transitions in Ne. The curves appear steeper than the cross sections shown in Fig. 1 due to the energy scale used. The computed values of  $df/d\epsilon$  have been used out to  $\epsilon = 10$  Ry. For higher energies two extrapolations were made assuming that  $df/d\epsilon \sim (\epsilon - \epsilon_{2p})^{-s}$  and that the extrapolated curve has the value computed at  $\epsilon = 10$ . The upper curves were determined by requiring that Eq. (15) be satisfied. This leads to  $s = 2.4$  and  $\int_0^\infty (\epsilon - \epsilon_{2p})(df/d\epsilon)d\epsilon = 11.32$  rather than the expectation value of 7.40. The lower curves were obtained by requiring that Eq. (16) be satisfied. This leads to

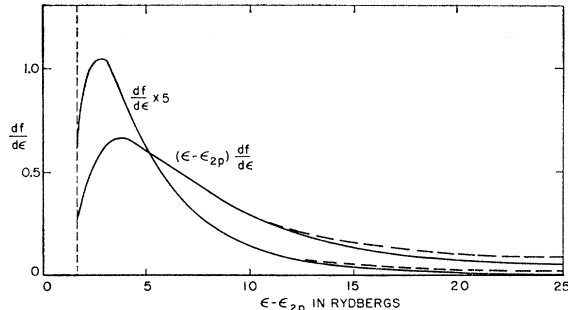


FIG. 10.  $df/d\epsilon$  and  $(\epsilon - \epsilon_{2p})df/d\epsilon$  for  $p \rightarrow d$  transitions in Ne.

$s = 2.9$  and  $\int_0^\infty (\epsilon - \epsilon_{2p})(df/d\epsilon)d\epsilon = 1.04$  rather than 1.11. The extrapolation could be done so that both sum rules are satisfied, but this is scarcely justified considering the numerical accuracy of the calculations. The numbers for the continuum contributions listed in Tables VII and VIII were based on a graphical extrapolation without any attempt to satisfy the sum rules. In Fig. 11 we show similar curves for  $df/d\epsilon$  and  $(\epsilon - \epsilon_{3p})df/d\epsilon$  corresponding to  $l \rightarrow l+1$  transitions in Ar. The curves show that the region  $\epsilon - \epsilon_{3p} > 3$  makes important contributions to the sums in Eqs. (15) and (16).

The sum rules (14)–(17) are special cases of more general rules which apply to transitions from a given state of an atomic system.<sup>39</sup> The more general rules are

$$\sum_n (E_0 - E_n)^{-1} f_{n0} = \frac{1}{3} \left( \left| \sum_i \mathbf{r}_i \right|^2 \right)_{00}, \quad (18)$$

$$\sum_n f_{n0} = Z, \quad (19)$$

$$\sum_n (E_0 - E_n) f_{n0} = \frac{4}{3} \left[ (E_0 + \frac{1}{2} \sum_{i \neq j} (\mathbf{p}_i \cdot \mathbf{p}_j)_{00}) \right], \quad (20)$$

$$\sum_n (E_0 - E_n)^2 f_{n0} = (16\pi Z/3) \sum_i [\delta^3(\mathbf{r}_i)]_{00}. \quad (21)$$

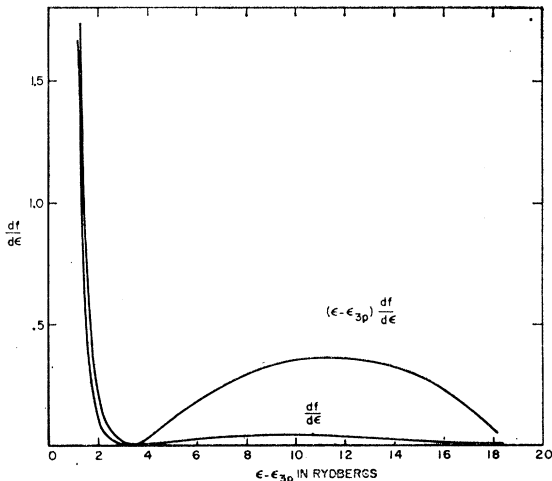


FIG. 11.  $df/d\epsilon$  and  $(\epsilon - \epsilon_{3p})df/d\epsilon$  for  $p \rightarrow d$  transitions in Ar.

<sup>39</sup> A. Dalgarno and N. Lynn, Proc. Phys. Soc. (London) A70, 802 (1957).

TABLE IX. Contributions to Equations (18)–(21).

	This paper	Dalgarno and Stewart <sup>a</sup>
Eq. (18)	0.763	0.7525
Eq. (19)	2	2
Eq. (20)	7.62	8.17
Eq. (21)	120.5	121.3

<sup>a</sup> See reference 28.

In the above  $f_{n0}$  is the oscillator strength for a transition from a given state 0 of energy  $E_0$  to a state  $n$  of energy  $E_n$ ,  $\mathbf{r}_i$ , and  $\mathbf{p}_i$  are the position and momentum vectors of the  $i$ th electron and  $Z$  is the atomic number. The more general formulas have so far only been applied to the case of He. Applications to heavier atoms are difficult for two reasons. First, for most atoms the only available ground-state wave functions are Hartree-Fock functions and evaluation of expectation values from these leads to a set corresponding to Eqs. (14)–(17) rather than to Eqs. (18)–(21). Second, the correlation term in Eqs. (18) and (20) of the form  $(\mathbf{r}_i \cdot \mathbf{r}_j)_{00}$  and  $(\mathbf{p}_i \cdot \mathbf{p}_j)_{00}$  will have the effect of mixing up contributions of the oscillator strength distribution from different atomic subshells.

For He there are no excluded states in the one-electron treatment and the correlation terms in the sum rules (18)–(21) are small. In Table IX we show a comparison of the central potential expectation values (for two electrons) corresponding to Eqs. (18)–(21) with the more accurate values given by Dalgarno and Stewart.<sup>28</sup> The close agreement of the expectation values based on the Hartree ground-state wave function with those computed from more accurate wave functions explains why our model gives such realistic results for the helium photoionization.

## VI. FINAL REMARKS

The preceding sections have shown that a simplified one-electron model based on the effective central potential obtained from Hartree-Fock ground-state orbitals provides a reasonably good first approximation to the oscillator strength spectral distribution for transitions from outer atomic subshells. Application of the model to inner subshells, while not made here, is straightforward. Thus, the model may be used to compute, in first approximation, the entire spectral distribution of oscillator strengths from a particular state of an atom. Such calculations, while lengthy, can easily be performed using present-day high-speed computers.

There seem to be three ways in which the methods of the present paper might be extended. The first, and in our opinion the least promising, is to perform calculations similar to those reported here using an effective central potential which has been modified in some manner to include effects neglected by our treatment. Some work has already been done along these lines

using semiempirical methods.<sup>40</sup> However, the accuracy of such calculations is difficult to estimate.

For light atoms, particularly Li and Be, calculations of ground-state wave functions which include estimates of the effects of electron correlation are available.<sup>41</sup> Using Eqs. (18)–(21) it is possible to obtain an estimate of the effects of electron correlation of the oscillator strength distribution for transitions from such states by evaluating the ground-state expectation parameters which appear on the right-hand side of these equations. While the mixing of contributions to the oscillator strength distribution from different subshells will make such an analysis difficult, such an approach is feasible, at least for Li and Be.

A third approach is to consider the central potential model described in this paper as an initial approximation, and to expand the wave functions for a particular state in the complete set of eigenstates pertaining to the central potential model. This approach has recently been formulated<sup>42</sup> in a way that is applicable to both discrete and continuum states. The application to photoionization and oscillator strength calculations, although complex, appears to be straightforward.

## ACKNOWLEDGMENT

A great deal of work reported here was done in collaboration with Dr. U. Fano. I would like to thank Dr. Fano for many helpful discussions and especially for a critical review of the manuscript.

## APPENDIX A

### Normalization of Continuum Wave Functions

For large  $r$  Eq. (4) is of the form

$$d^2P_{el}/dr^2 + A(r)P_{el} = 0, \quad (A1)$$

$$A(r) = -\frac{2}{r} + \epsilon - \frac{l(l+1)}{r^2}. \quad (A2)$$

We assume that in the range where  $A(r)$  is of the form given by (A2) that an unnormalized solution  $P_{el}$  may be represented as

$$P_{el} = C(\pi x)^{-1/2} \sin \theta(r), \quad (A3)$$

where

$$x = d\theta/dr$$

and  $C$  is the normalization constant. From (A1) and (A3) we have

$$x^2 = A(r) + x^{-1/2} d^2(x^{-1/2})/dr^2. \quad (A4)$$

<sup>40</sup> See, for example, L. Bierman and K. Lubeck, Z. Astrophys. 25, 325 (1948) and A. S. Douglas, Proc. Cambridge Phil. Soc. 52, 687 (1956).

<sup>41</sup> See A. Weiss, Phys. Rev. 122, 1826 (1961) and references contained therein.

<sup>42</sup> U. Fano and F. Prats, J. Natl. Acad. Sci. (India), (to be published).

For large  $r$   $x \rightarrow \epsilon^{1/2}$  so a good approximation to  $x$  is obtained by a first-order iteration of (A4). This gives

$$x^2 \approx A - A^{-3/2} A''/4 + \frac{5}{16} (A')^2 A^{-5/2}, \quad (A5)$$

where the primes denote differentiation with respect to  $r$ .

Next we consider the solution given by (A3) at two points  $r_1$  and  $r_2$  and define the following quantities:

$$a_1 = x^{\frac{1}{2}}(r_1) P_{el}(r_1) = \pi^{-\frac{1}{2}} C \sin\theta(r_1), \quad (A6)$$

$$a_2 = x^{\frac{1}{2}}(r_2) P_{el}(r_2) = \pi^{-\frac{1}{2}} C \sin\theta(r_2), \quad (A7)$$

$$\alpha = \int_{r_1}^{r_2} x dr = \theta(r_2) - \theta(r_1). \quad (A8)$$

(A6), (A7), and (A8) may be solved for  $C$  in terms of  $a_1$ ,  $a_2$ , and  $\alpha$ . The result is

$$C = \pi^{1/4} [(a_1^2 + a_2^2 - 2a_1 a_2 \cos\alpha) / \sin^2\alpha]^{1/2}. \quad (A9)$$

(A9) may be used to evaluate the normalization constant  $C$  using the first-order solution (A5) for  $x$  and the values of the unnormalized wave function  $P_{el}$  at any two points. The procedure fails for values of  $\alpha = n\pi$ , but apart from this restriction was found to be quite unsensitive to the choice of  $r_1$  and  $r_2$ . Since the formulas involved are simple, the computer coding was arranged so that  $C$  was computed for a number of values of  $r_1$  and  $r_2$ . Three-place accuracy in the values of  $C$  computed was obtained in practically all cases.